Available online at www.sciencedirect.com
ScienceDirect
Journal of Sound and Vibration 303 (2007) 154–170
JOURNAL OF SOUND AND VIBRATION
www.elsevier.com/locate/jsvi

Vibrations of circular cylindrical shells: Theory and experiments

Francesco Pellicano*

Dipartimento di Ingegneria Meccanica e Civile, Università di Modena e Reggio Emilia, V. Vignolese 905, 41100 Modena, Italy

Received 17 March 2006; received in revised form 30 November 2006; accepted 3 January 2007
Available online 23 March 2007

Abstract

In the present paper, a method for analysing linear and nonlinear vibrations of circular cylindrical shells having different boundary conditions is presented; the method is based on the Sanders–Koiter theory. Displacement fields are expanded in a mixed double series based on harmonic functions and Chebyshev polynomials. Simply supported and clamped–clamped boundary conditions are analysed, as well as connections with rigid bodies; in the latter case experiments are carried out. Comparisons with experiments and finite-element analyses show that the technique is computationally efficient and accurate in modelling linear vibrations of shells with different boundary conditions.

An application to large amplitude of vibration shows that the technique is effective also in the case of nonlinear vibration: comparisons with the literature confirm the accuracy of the approach.

The method proposed is a general framework suitable for analysing vibration of circular cylindrical shells both in the case of linear and nonlinear vibrations.

1. Introduction

The continuous growing of the commercial use of Space facilities has led to the development of new and more efficient aerospace vehicles; therefore, new and accurate studies on light-weight, thin-walled structures are needed. A wide part of the technical literature in the past century was focalized on the analysis of thin-walled structures and tried to investigate their behaviour in many different operating conditions, i.e. under static or dynamic loads, either in presence or absence of fluid–structure interaction. Both linear and nonlinear models have been developed to forecast the response of such structures. Many studies were concerned with cylindrical shells that constitute main parts of aircrafts, rockets, missiles and generally aerospace structures.

The literature about vibration of shells is extremely wide and the reader can refer to Leissa [1] or more recently to Amabili and Païdoussis [2] for a comprehensive review of models and results present in literature. In the following, some studies, strictly related to the present paper, are described.

Liew et al. [3] analysed linear vibrations of shallow conical shells, using two-dimensional orthogonal polynomials and the Ritz procedure, for obtaining frequencies and modes of vibration: the approach was mesh-free and able to handle complex geometries and boundary conditions.

*Tel.: +39 059 2056154; fax: +39 059 2056129.
E-mail address: francesco.pellicano@unimore.it.

0022-460X/$ - see front matter © 2007 Elsevier Ltd. All rights reserved.
doi:10.1016/j.jsv.2007.01.022

Bhaskar and Dumir [4] analysed the dynamics of rectangular orthotropic plates, resting on a nonlinear elastic foundation: they used a discretization approach based on polynomials and orthogonal point collocation method, obtained from zeros of Legendre polynomials. The nonlinear dynamics was analysed by means of the averaging method and backbone curves were obtained.

Liew et al. [5] analysed conical shells by means of a mesh-free approach based on the Ritz method and a mixed Fourier-polynomial expansion. They considered both simply supported and clamped boundary conditions. The same authors used the same approach for analysing laminated cylindrical panels [6].

Zhou et al. [7] developed an approach based on Chebyshev polynomials and Ritz method for evaluating natural frequencies of solid and hollow cylinders. Soldatos and Messina [8] used orthogonal polynomials for analysing laminated circular cylinders.

Ng et al. [9] studied parametric instabilities of conical shells, using the generalized differential quadrature method, which has been proven to be quite effective for linear problems; in such a work instability regions were evaluated by means of the Bolotin approach, but the study did not consider either dissipation or postcritical nonlinear vibrations. A similar approach was used in Ref. [10] for studying linear free vibrations of conical panels.

Nayfeh and Arafat [11] analysed nonlinear axisymmetric vibrations of spherical shells, by means of Legendre polynomials for spatial discretizations, and multiple scale method for the dynamic scenario.

A special comment deserves the work of Trotsenko and Trotsenko [12], who studied vibrations of circular cylindrical shells with attached rigid bodies, by means of an approach quite close to the present theory. In Ref. [12], the authors used a mixed expansion based on trigonometric functions and Legendre polynomials; they considered only linear vibrations. One of these authors published recently a paper on the same subject [13], in which results and theory present in Ref. [12] are reprinted (such work is cited for completeness).

The literature analysis shows that in the past several methods were developed for investigating: (i) linear vibrations of complex shells; (ii) nonlinear vibrations of shells having simple shape and boundary conditions. Therefore, a contribution toward developing a general framework that allows to study the aforementioned items is welcome. The present work is a contribution in such direction.

In the present paper, linear and nonlinear vibrations of circular cylindrical shells are analysed. Sanders–Koiter theory is considered for shell modelling; in this theory, the shell deformation is described in terms of three displacements fields (longitudinal, circumferential and radial); geometric nonlinearities due to large amplitude of vibration are modelled. Displacement fields are expanded by means of a double mixed series: harmonic functions for the circumferential variable; Chebyshev polynomials for the longitudinal variable. Then Lagrange equations are considered to obtain a system of ordinary differential equations, from potential and kinetic energies and the virtual work of external forces.

Simply supported and clamped–clamped configurations are analysed in detail, both comparing the present theory with exact solutions (for simply supported shells only) and finite elements. Moreover, a shell, clamped at the base and connected to a rigid body, is analysed experimentally, analytically (present theory) and using standard finite-elements models. The experimental set-up is described as well as the experimental analysis, which includes frequency, damping and mode shape identification.

Nonlinear vibrations, due to large amplitude of vibration, are analysed in the case of simply supported shells; the present theory is compared with the literature.

2. Equations of motion

In Fig. 1 a circular cylindrical shell having radius R, length L and thickness h is represented; a cylindrical coordinate system $(O; x, r, \theta)$ is considered in order to take advantage from the axial symmetry of the structure, the origin of the reference system is located at the centre of one end of the shell. In Fig. 1 three displacement fields are represented: axial $u(x, \theta, t)$, circumferential $v(x, \theta, t)$ and radial $w(x, \theta, t)$.

Geometric imperfections can be considered in the theory by means of an initial radial displacement field $w_0(x, \theta)$; however, in the numerical results, only perfect shells are considered.

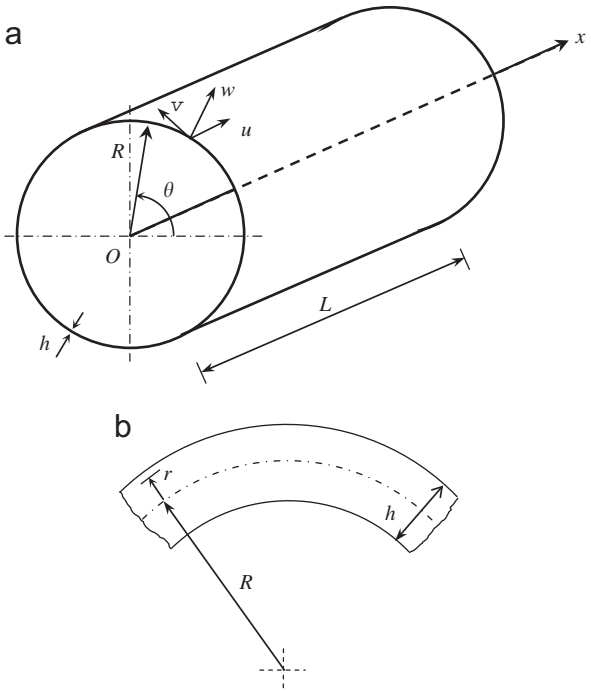

Fig. 1. Circular cylindrical shell: coordinate system and dimensions. (a) Complete shell; (b) cross-section of the shell surface.

2.1. Strain energy

The Sanders–Koiter theory is based on Love's first approximation: (i) $h \ll R$; (ii) strains are small; (iii) transverse normal stresses are small; and (iv) the normal to the undeformed middle surface remains straight and normal to the middle surface after deformation, no thickness stretching is present (Kirchhoff–Love kinematic hypothesis) [1,2,14]; (v) rotary inertia and shear deformations are neglected.

It is interesting to report comments of Leissa [1] about the accuracy of the Sanders–Koiter theory and generally about theories that are based on the first Love hypothesis: "for very thin shells ($R/h = 500$), all theories are in closer agreement than for thicker shells ($R/h = 20$), for very short shells ($L/(mR) = 0.1, 0.25$) none of the shell theories compare favourably with 3D elasticity"; further and deeper comments can be found in Ref. [1], p. 49.

Strain components ε_x, ε_θ and $\gamma_{x\theta}$ at an arbitrary point of the shell are [1]

$$\varepsilon_x = \varepsilon_{x,0} + rk_x, \quad \varepsilon_\theta = \varepsilon_{\theta,0} + rk_\theta, \quad \gamma_{x\theta} = \gamma_{x\theta,0} + rk_{x\theta}, \tag{1}$$

where $\varepsilon_{x,0}$, $\varepsilon_{\theta,0}$ and $\gamma_{x\theta,0}$ are middle surface strains; k_x, k_θ and $k_{x\theta}$ are curvature and torsion changes of the middle surface; and r is the distance of the arbitrary point of the shell from the middle surface (see Fig. 1(b)).

According to the Sanders–Koiter theory, middle surface strains and changes in the curvature and torsion are given by [1,2]

$$\varepsilon_{x,0} = \frac{\partial u}{L\partial\eta} + \frac{1}{2}\left(\frac{\partial w}{L\partial\eta}\right)^2 + \frac{1}{8}\left(\frac{\partial v}{L\partial\eta} - \frac{\partial u}{R\partial\theta}\right)^2 + \frac{\partial w}{L\partial\eta}\frac{\partial w_0}{L\partial\eta}, \tag{2a}$$

$$\varepsilon_{\theta,0} = \frac{\partial v}{R\partial\theta} + \frac{w}{R} + \frac{1}{2}\left(\frac{\partial w}{R\partial\theta} - \frac{v}{R}\right)^2 + \frac{1}{8}\left(\frac{\partial u}{R\partial\theta} - \frac{\partial v}{L\partial\eta}\right)^2 + \frac{\partial w_0}{R\partial\theta}\left(\frac{\partial w}{R\partial\theta} - \frac{v}{R}\right), \tag{2b}$$

$$\gamma_{x\theta,0} = \frac{\partial u}{R\partial\theta} + \frac{\partial v}{L\partial\eta} + \frac{\partial w}{L\partial\eta}\left(\frac{\partial w}{R\partial\theta} - \frac{v}{R}\right) + \frac{\partial w_0}{L\partial\eta}\left(\frac{\partial w}{R\partial\theta} - \frac{v}{R}\right) + \frac{\partial w}{L\partial\eta}\frac{\partial w_0}{R\partial\theta}, \tag{2c}$$

$$k_x = -\frac{\partial^2 w}{L^2\,\partial\eta^2}, \quad k_\theta = \frac{\partial v}{R^2\,\partial\theta} - \frac{\partial^2 w}{R^2\,\partial\theta^2}, \quad k_{x\theta} = -2\frac{\partial^2 w}{LR\,\partial\eta\,\partial\theta} + \frac{1}{2R}\left(3\frac{\partial v}{L\,\partial\eta} - \frac{\partial u}{R\,\partial\theta}\right), \tag{2d}$$

where $\eta = x/L$ is the nondimensional longitudinal coordinate.

In Eqs. (2a)–(c), nonlinear terms become important when the amplitude of vibration is of the order of the shell thickness [1,2].

The elastic strain energy U_S of a circular cylindrical shell, neglecting the radial stress σ_r (Love's first approximation), is given by [14]

$$U_S = \frac{1}{2}LR\int_0^{2\pi}\int_0^1\int_{-h/2}^{h/2}(\sigma_x\varepsilon_x + \sigma_\theta\varepsilon_\theta + \tau_{x\theta}\gamma_{x\theta})\,\mathrm{d}\eta(1 + r/R)\,\mathrm{d}\theta\,\mathrm{d}r. \tag{3}$$

In the case of homogeneous and isotropic materials, stresses σ_x, σ_θ and $\tau_{x\theta}$ are related to strains ($\sigma_r = 0$, case of plane stress) [14]

$$\sigma_x = \frac{E}{1-\nu^2}(\varepsilon_x + \nu\varepsilon_\theta), \quad \sigma_\theta = \frac{E}{1-\nu^2}(\varepsilon_\theta + \nu\varepsilon_x), \quad \tau_{x\theta} = \frac{E}{2(1+\nu)}\gamma_{x\theta}, \tag{4}$$

where E is the Young's modulus and ν is the Poisson's ratio.

Using Eqs. (1), (3), (4), the following expression of the potential energy is obtained:

$$\begin{aligned} U_S = {} & \frac{1}{2}\frac{Eh}{1-\nu^2}LR\int_0^{2\pi}\int_0^1\left(\varepsilon_{x,0}^2 + \varepsilon_{\theta,0}^2 + 2\nu\varepsilon_{x,0}\varepsilon_{\theta,0} + \frac{1-\nu}{2}\gamma_{x\theta,0}^2\right)\mathrm{d}\eta\,\mathrm{d}\theta \\ & + \frac{1}{2}\frac{Eh^3}{12(1-\nu^2)}LR\int_0^{2\pi}\int_0^1\left(k_x^2 + k_\theta^2 + 2\nu k_x k_\theta + \frac{1-\nu}{2}k_{x\theta}^2\right)\mathrm{d}\eta\,\mathrm{d}\theta + O(h^4), \end{aligned} \tag{5}$$

where $O(h^4)$ is a higher-order term in h according to the Sanders–Koiter theory.

The first term of the right-hand side of Eq. (5) is the membrane energy (also referred to stretching) and the second one is the bending energy.

The kinetic energy T_S of a circular cylindrical shell (rotary inertia is neglected) is given by

$$T_S = \frac{1}{2}\rho_S hLR\int_0^{2\pi}\int_0^1(\dot{u}^2 + \dot{v}^2 + \dot{w}^2)\,\mathrm{d}\eta\,\mathrm{d}\theta, \tag{6}$$

where ρ_s is the mass density of the shell, the overdot denotes a time derivative.

The virtual work W done by the external forces is written as

$$W = LR\int_0^{2\pi}\int_0^1(q_x u + q_\theta v + q_r w)\mathrm{d}\eta\,\mathrm{d}\theta, \tag{7}$$

where q_x, q_θ and q_r are the distributed forces per unit area acting in axial, circumferential and radial directions, respectively.

In-plane forces and bending moments depend on the shell strain; in the following, only relationships used in applying boundary conditions are reported:

$$M_x = \frac{Eh^3}{12(1-\nu^2)}(k_x + \nu k_\theta), \quad N_x = \frac{Eh}{1-\nu^2}(\varepsilon_{x,0} + \nu\varepsilon_{\theta,0}). \tag{8}$$

3. Linear vibration: modal analysis

In order to carry out a linear vibration analysis, in the present section, linear Sanders–Koiter theory is considered, i.e. in Eq. (5), only quadratic terms are retained.

The best basis for expanding displacement fields is the eigenfunction basis, but only for special boundary conditions such basis can be found analytically; generally, eigenfunctions must be evaluated in an approximate way.

In order to attack the general problem of circular cylindrical shell vibration, displacement fields are expanded by means of a double series: the axial symmetry of the geometry and the periodicity of the deformation in the circumferential direction, lead to use harmonic functions; Chebyshev polynomials are considered in the axial direction.

Let us now consider a modal vibration, i.e. a synchronous motion:

$$u(\eta,\theta,t)=U(\eta,\theta)f(t),\quad v(\eta,\theta,t)=V(\eta,\theta)f(t),\quad w(\eta,\theta,t)=W(\eta,\theta)f(t), \tag{9}$$

where $U(\eta,\theta)$, $V(\eta,\theta)$ and $W(\eta,\theta)$ represent the modal shape.

The modal shape is now expanded in a double series, in terms of Chebyshev polynomials $T_m^*(\eta)$ and harmonic functions:

$$U(\eta,\theta)=\sum_{m=0}^{M_U}\sum_{n=0}^{N}\tilde{U}_{m,n}T_m^*(\eta)\cos n\theta, \tag{10a}$$

$$V(\eta,\theta)=\sum_{m=0}^{M_V}\sum_{n=0}^{N}\tilde{V}_{m,n}T_m^*(\eta)\sin n\theta, \tag{10b}$$

$$W(\eta,\theta)=\sum_{m=0}^{M_W}\sum_{n=0}^{N}\tilde{W}_{m,n}T_m^*(\eta)\cos n\theta, \tag{10c}$$

where $T_m^*(\eta)=T_m(2\eta-1)$ and $T_m(\cdot)$ is the mth-order Chebyshev polynomial [15].

Note that, in absence of imperfections, a linear mode has the following simplified expression:

$$U(\eta,\theta)=\sum_{m=0}^{M_U}\tilde{U}_{m,n}T_m^*(\eta)\cos n\theta,\quad V(\eta,\theta)=\sum_{m=0}^{M_V}\tilde{V}_{m,n}T_m^*(\eta)\sin n\theta,\quad W(\eta,\theta)=\sum_{m=0}^{M_W}\tilde{W}_{m,n}T_m^*(\eta)\cos n\theta. \tag{11}$$

Expansions (10) or (11) do not satisfy any particular boundary condition.

3.1. Boundary conditions

In the present work, boundary conditions are considered by applying constraints to the free coefficients of expansions (10a–c) or (11). Some of the coefficients $\tilde{U}_{m,n}$, $\tilde{V}_{m,n}$ and $\tilde{W}_{m,n}$ of Eqs. (10a–c) or (11), can be suitably chosen in order to satisfy boundary conditions.

The approach is explained by means of examples, in order to show the intrinsic simplicity of the method as well as the capability of handling complex boundary conditions.

3.1.1. Simply supported

The following boundary conditions are imposed to the mode shape:

$$w=0, v=0,\quad M_x=0,\quad N_x=0\quad \text{for } \eta=0,1, \tag{12}$$

which imply

$$W(\eta,\theta)=\sum_{m=0}^{M_W}\sum_{n=0}^{N}\tilde{W}_{m,n}T_m^*(\eta)\cos n\theta=0\quad \text{for } \eta=0,1, \tag{13a}$$

$$V(\eta,\theta)=\sum_{m=0}^{M_V}\sum_{n=0}^{N}\tilde{V}_{m,n}T_m^*(\eta)\sin n\theta=0\quad \text{for } \eta=0,1, \tag{13b}$$

$$W_{,\eta\eta}(\eta,\theta)=\sum_{m=0}^{M_W}\sum_{n=0}^{N}\tilde{W}_{m,n}T_{m,\eta\eta}^*(\eta)\cos n\theta=0\quad \text{for } \eta=0,1, \tag{13c}$$

$$U_{,\eta}(\eta,\theta)=\sum_{m=0}^{M_U}\sum_{n=0}^{N}\tilde{U}_{m,n}T^{*}_{m,\eta}(\eta)\cos n\theta=0 \quad \text{for } \eta=0,1, \tag{13d}$$

where $(\cdot)_{,\eta}=\partial(\cdot)/\partial\eta$ and $(\cdot)_{,\eta\eta}=\partial^2(\cdot)/\partial\eta^2$.

Such conditions are valid for any θ and n; therefore, Eqs. (13a–d) are modified as follows:

$$\sum_{m=0}^{M_W}\tilde{W}_{m,n}T^{*}_{m}(\eta)=0, \quad \sum_{m=0}^{M_V}\tilde{V}_{m,n}T^{*}_{m}(\eta)=0, \quad \sum_{m=0}^{M_W}\tilde{W}_{m,n}T^{*}_{m,\eta\eta}(\eta)=0,$$
$$\sum_{m=0}^{M_U}\tilde{U}_{m,n}T^{*}_{m,\eta}(\eta)=0, \quad n=0,1,\ldots \quad \text{for } \eta=0,1. \tag{14}$$

The linear algebraic system of Eq. (14) is solved in terms of the coefficients: $\tilde{U}_{1,n}$, $\tilde{U}_{2,n}$, $\tilde{V}_{0,n}$, $\tilde{V}_{1,n}$, $\tilde{W}_{0,n}$, $\tilde{W}_{1,n}$, $\tilde{W}_{2,n}$, $\tilde{W}_{3,n}$, $n=0,1,\ldots$; which can be obtained exactly in terms of the remaining unknown coefficients. In the present work, the solution of system (14) is carried out by means of an algebraic manipulation software.

3.1.2. Clamped–clamped

The following boundary conditions are imposed to the mode shape:

$$w=0, \quad w_{,\eta\eta}=0, \quad v=0, \quad u=0 \quad \text{for } \eta=0,1. \tag{15}$$

The procedure is formally the same of simply supported boundary conditions; however, the resulting linear system is solved in terms of the following coefficients: $\tilde{U}_{0,n}$, $\tilde{U}_{1,n}$, $\tilde{V}_{0,n}$, $\tilde{V}_{1,n}$, $\tilde{W}_{0,n}$, $\tilde{W}_{1,n}$, $\tilde{W}_{2,n}$, $\tilde{W}_{3,n}$, $n=0,1,\ldots$

3.1.3. Clamped-disk-on-the-top

In this case both theoretical, experimental and finite-elements analyses are carried out; therefore, a particular system is considered, in Fig. 2 the geometry of the system as well as the dimensions are represented, the scheme corresponds to the experimental set-up of Fig. 3.

The shell is clamped at the bottom to a rigid support; therefore, for $\eta=0$ the boundary conditions are the same of the clamped–clamped case, Eq. (15).

In order to impose boundary conditions to the top end of the shell, it is useful to consider the rigid body motion of the disk. Such a body has six degrees of freedom (dof's); however, in the present work torsional vibration is not considered; therefore, the number of dof's is reduced to five. Moreover, experiments evidenced that the rigid body motion presents extremely small amplitude; therefore, a linearized analysis of the disk motion will be performed in the following. Rigid body (disk) dof's are additional variables of the problem, in writing boundary conditions of the shell top end, the rigid body motion is considered as an imposed displacement.

Let us consider a Cartesian reference system (O', x', y', z') having the origin located at the centre of the shell top end ($\eta=1$), see Fig. 4; note that the origin of the circumferential coordinate θ (Fig. 1) is set coincident with axis y' (Fig. 4). S_{Dx}, S_{Dy}, S_{Dz} are three displacement components of the motion of the origin (O'), see Fig. 4. The rotation is treated in a simplified way: the small amplitude of the body motion allows to linearize the analysis and to apply the superposition principle; the global rotation is assumed to be a superposition of three rotations about three axes (x', y', z').

Given an arbitrary and infinitesimal motion to the top disk, Fig. 4, and considering the shell clamped to the disk, one obtains the following boundary conditions:

$$u(L,\theta,t)=-R\alpha_y(t)\sin\theta-R\alpha_z(t)\cos\theta+S_{Dx}(t), \tag{16a}$$

$$v(L,\theta,t)=-S_{Dy}(t)\sin\theta-S_{Dz}(t)\cos\theta-R\alpha_x(t), \tag{16b}$$

$$w(L,\theta,t)=S_{Dy}(t)\cos\theta-S_{Dz}(t)\sin\theta, \tag{16c}$$

$$\theta_\alpha=-\alpha_y(t)\sin\theta-\alpha_z(t)\cos\theta, \tag{16d}$$

where $\theta_\alpha=-(1/L)(\partial w/\partial\eta)|_{x=L}$.

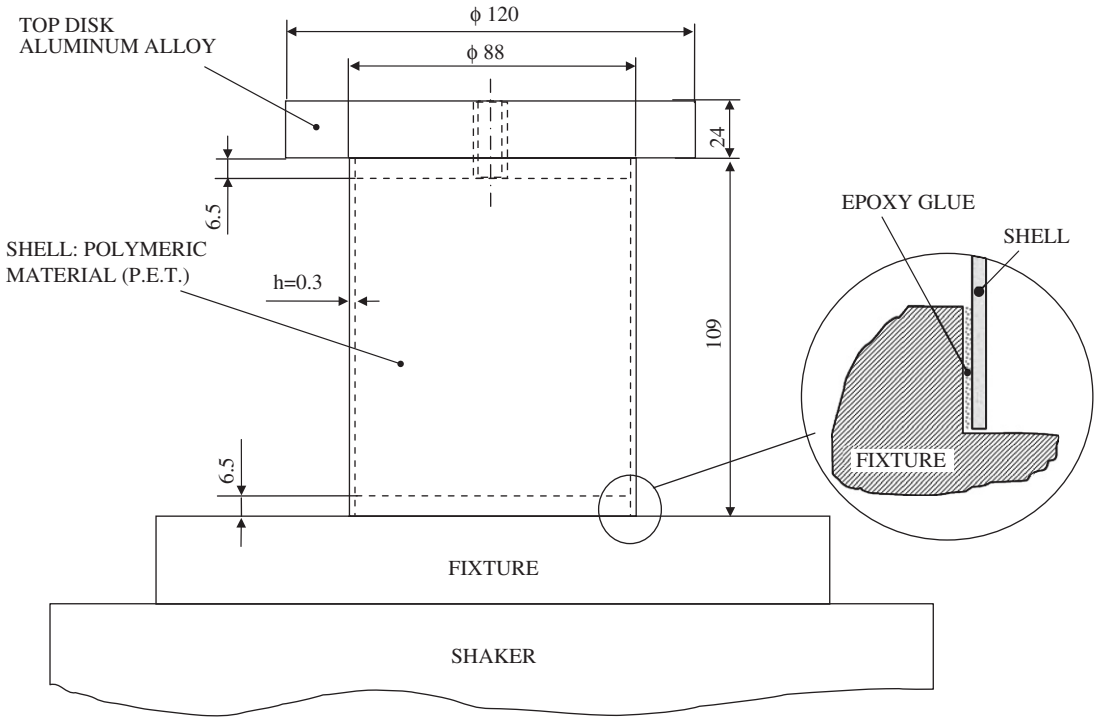

Fig. 2. Configuration and dimensions (millimiters) of the system analysed experimentally.

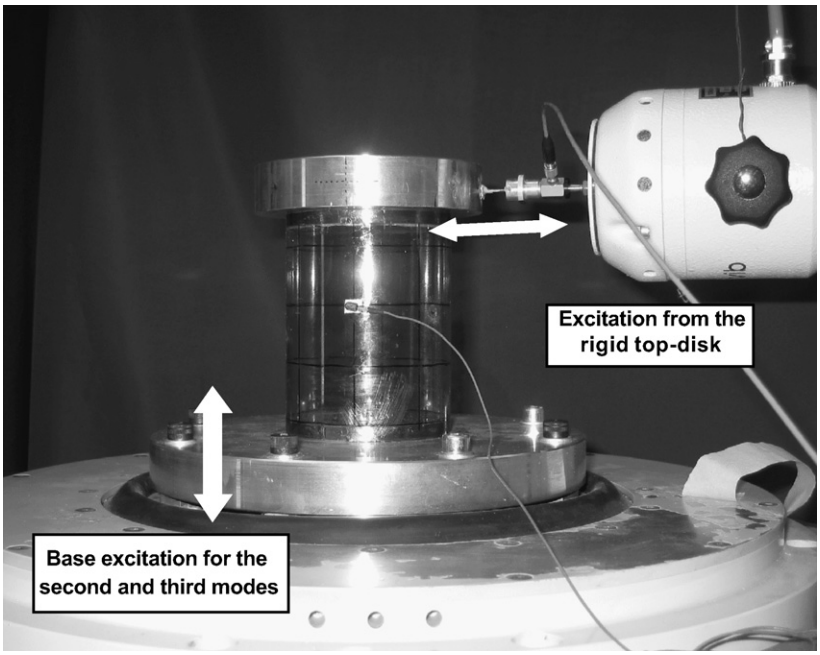

Fig. 3. Experimental set-up and excitation types.

Note that Eqs. (16a–d) are in agreement with Ref. [12], where such conditions are obtained by means of a different approach.

It is to note that, for $n>1$ boundary conditions given by the rigid body motion correspond to clamping (see Eq. (14)); moreover, axisymmetric modes ($n=0$) are influenced by S_{Dx} only.

3.2. Kinetic energy: disk on the top

The kinetic energy of the shell is given by Eq. (6); when a rigid body is connected to one of the shell ends, its kinetic energy must be added to the shell energy.

A rigid body motion, imposed to the shell top end, induces a motion of the top disk; in particular, the motion of its centre of mass G depends both on the displacement of O' and two rotations (see Figs. 4 and 5). Assuming also infinitesimal rotations and linearizing all relationships, one easily obtains:

$$x_G(t) = S_{Dx}(t), \quad y_G(t) = S_{Dy}(t) + \alpha_z(t)h_G, \quad z_G(t) = S_{Dz}(t) - \alpha_y(t)h_G. \tag{17}$$

If one is not interested in torsional vibrations of the shell, the rotation about x'-axis can be neglected; therefore, the kinetic energy of the disk is given by

$$T_D = \tfrac{1}{2}m_D(\dot{S}_{Dy} + \dot{\alpha}_z h_G)^2 + \tfrac{1}{2}m_D(\dot{S}_{Dz} - \dot{\alpha}_y h_G)^2 + \tfrac{1}{2}J_z\dot{\alpha}_z^2 + \frac{1}{2}J_y\dot{\alpha}_y^2 + \frac{1}{2}m_D\dot{S}_{Dx}^2. \tag{18}$$

3.3. Discretization: Lagrange equations

Eq. (9) and expansions (10) are inserted in the expressions of the kinetic and the potential energy (for the linear system); then a set of ordinary differential equations is obtained by using Lagrange equations.

An intermediate step is the reordering of variables, in order to proceed in a systematic way. A vector containing all variables is built depending on the boundary conditions.

Simply supported:

$$\mathbf{q} = [\tilde{U}_{0,0}, \tilde{U}_{3,0}, \tilde{U}_{4,0}, \ldots, \tilde{U}_{0,1}, \tilde{U}_{3,1}, \tilde{U}_{4,1}, \ldots, \tilde{V}_{2,0}, \tilde{V}_{3,0}, \ldots, \tilde{V}_{2,1}, \tilde{V}_{3,1}, \ldots, \tilde{W}_{4,0}, \tilde{W}_{5,0}, \ldots, \tilde{W}_{4,1}, \tilde{W}_{5,1}, \ldots,]f(t), \tag{19}$$

Clamped–clamped:

$$\mathbf{q} = [\tilde{U}_{2,0}, \tilde{U}_{3,0}, \ldots, \tilde{U}_{2,1}, \tilde{U}_{3,1}, \ldots, \tilde{V}_{2,0}, \tilde{V}_{3,0}, \ldots, \tilde{V}_{2,1}, \tilde{V}_{3,1}, \ldots, \tilde{W}_{4,0}, \tilde{W}_{5,0}, \ldots, \tilde{W}_{4,1}, \tilde{W}_{5,1}, \ldots,]f(t), \tag{20}$$

Rigid body connected to the shell:

$$\mathbf{q} = [\tilde{U}_{2,0}, \tilde{U}_{3,0}, \ldots, \tilde{U}_{2,1}, \tilde{U}_{3,1}, \ldots, \tilde{V}_{2,0}, \tilde{V}_{3,0}, \ldots, \tilde{V}_{2,1}, \tilde{V}_{3,1}, \ldots, \tilde{W}_{4,0}, \tilde{W}_{5,0}, \ldots, \tilde{W}_{4,1}, \tilde{W}_{5,1}, \ldots, \tilde{S}_{Dx}, \tilde{S}_{Dy}, \tilde{S}_{Dz}, \tilde{\alpha}_y, \tilde{\alpha}_z]f(t), \tag{21}$$

where $S_{Dx} = f(t)\tilde{S}_{Dx}$, $S_{Dy} = f(t)\tilde{S}_{Dy}$, $S_{Dz} = f(t)\tilde{S}_{Dz}$, $\alpha_y = f(t)\tilde{\alpha}_y$, $\alpha_z = f(t)\tilde{\alpha}_z$.

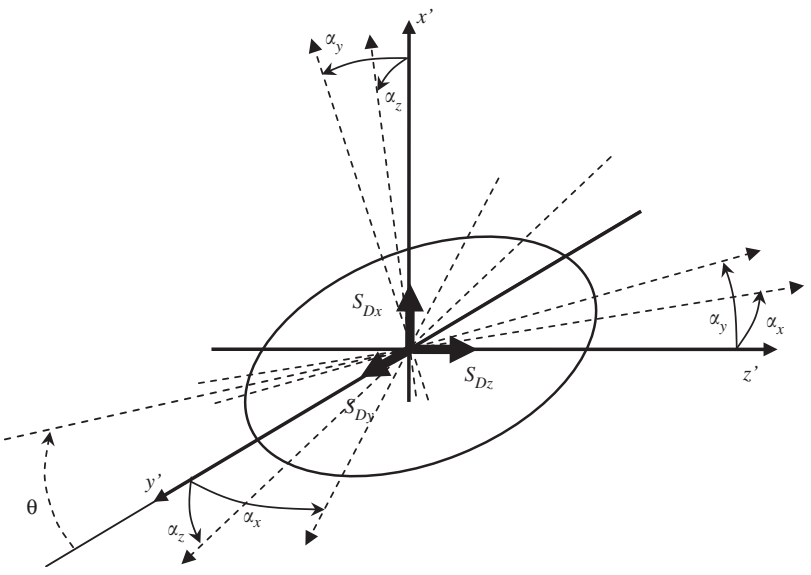

Fig. 4. Rigid body motion imposed at the top shell end ($\eta = 1$).

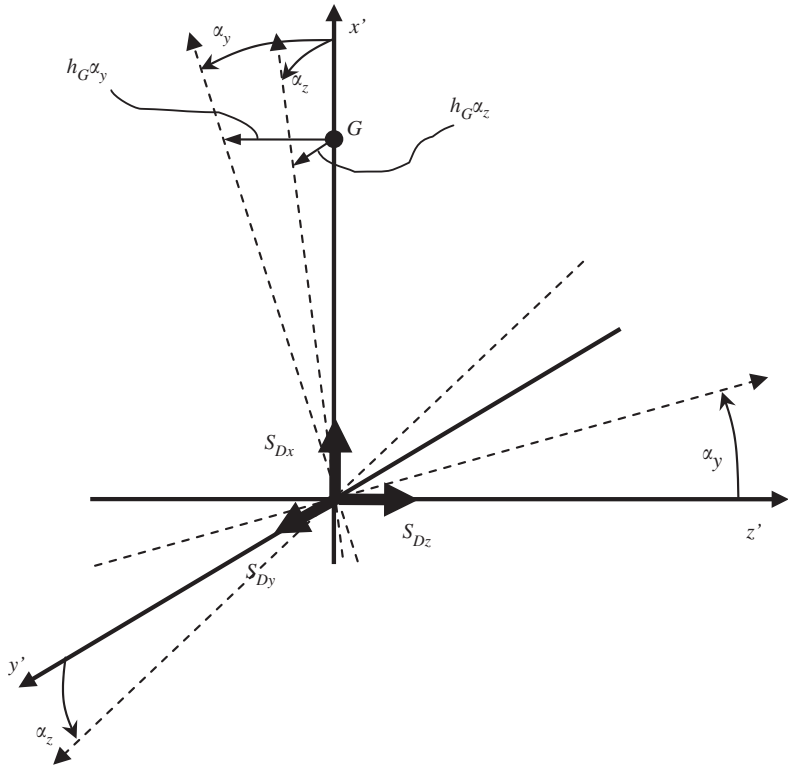

Fig. 5. Displacement of the top disk centre of mass, due to a rigid body motion of the shell-top end.

Note that the torsional dof of the disk is neglected in the present paper; therefore, α_x is not included in Eq. (21). Moreover, a unique time law $f(t)$ is considered in order to impose a synchronous motion (modal vibration); such assumption will be relaxed in the case of nonlinear vibration.

The maximum number of variables needed for describing a generic mode with n nodal diameters is: $N_P = M_U + M_V + M_W - 5$ without connected rigid body and $N_P = M_U + M_V + M_W$ with the rigid body.

Lagrange equations for free vibrations are

$$\frac{\mathrm{d}}{\mathrm{d}t}\left(\frac{\partial L}{\partial \dot{q}_i}\right) - \frac{\partial L}{\partial q_i} = 0, \quad i = 1, 2, \ldots, N_{\max}, \tag{22}$$

where $L = T - U_S$; $T = T_S + T_D$ and $N_{\max} = N_P \times N$.

Using Eq. (19) and considering a harmonic motion, $f(t) = \mathrm{e}^{\mathrm{j}\omega t}$, one obtains:

$$(-\omega^2 \mathbf{M} + \mathbf{K})\mathbf{q} = \mathbf{0} \tag{23}$$

which is the classical nonstandard eigenvalue problem that furnishes frequencies and modes of vibration (eigenvalues and eigenvectors).

A modal shape corresponding to the jth mode is given by Eqs. (10a–c); where: $\tilde{U}_{m,n}$, $\tilde{V}_{m,n}$ and $\tilde{W}_{m,n}$ are substituted with $\tilde{U}^{(j)}_{m,n}$, $\tilde{V}^{(j)}_{m,n}$ and $\tilde{W}^{(j)}_{m,n}$, which are components of the jth eigenvector of Eq. (23) and the vector function $\mathbf{U}^{(j)}(x,\theta) = [U^{(j)}(x,\theta), V^{(j)}(x,\theta), W^{(j)}(x,\theta)]^{\mathrm{T}}$ is the jth eigenfunction vector of the original problem.

Eigenfunctions are normalized by imposing that $\max[\max[U^{(j)}(x,\theta)], \max[V^{(j)}(x,\theta)], \max[W^{(j)}(x,\theta)]] = 1$; the physical meaning of such normalization is the following: the modal coordinate $f_i(t)$ represents the maximum amplitude of vibration referred to the dominant direction of a mode shape (radial w, circumferential v or longitudinal u). For example, in the case of radial dominant modes, in the eigenfunction vector $\mathbf{U}^{(j)}(x,\theta)$ the third component will have a maximum amplitude much larger than the others; if we

normalize the vector function in order to have such maximum equal to 1, then $f_i(t)$ will give the maximum amplitude of vibration in the radial direction.

The present normalization is particularly useful in nonlinear analyses; in particular, it improves numerical accuracy and efficiency and improves the results interpretation.

4. Nonlinear analysis

In the nonlinear analysis the full expression of potential shell energy (5), containing terms up to fourth order (cubic nonlinearity), is considered. Displacement fields $u(x, \theta, t)$, $v(x, \theta, t)$ and $w(x, \theta, t)$ are expanded by using linear mode shapes obtained in the previous section:

$$u(x,\theta,t)=\sum_{j=1}^{N_{\max}} U^{(j)}(x,\theta) f_{u,j}(t), \quad v(x,\theta,t)=\sum_{j=1}^{N_{\max}} V^{(j)}(x,\theta) f_{v,j}(t),$$
$$w(x,\theta,t)=\sum_{j=1}^{N_{\max}} W^{(j)}(x,\theta) f_{w,j}(t). \tag{24}$$

Expansions (24) respect the boundary conditions, modal shapes $U^{(j)}(x,\theta)$, $V^{(j)}(x,\theta)$, $W^{(j)}(x,\theta)$, are known functions expressed in terms of polynomials and harmonic functions. It is to note that in Eq. (24) the time function is different for each displacement field; therefore, expansion (24) is an extension of expansion (9) and apparently it increases the number of dof's of the system. Conversely, using expansion (24) one can select suitable shapes for each displacement field separately, improving the convergence speed, reducing the number of dof's and increasing the computational accuracy.

Expansion (24) is put in the strain and kinetic energy (Eqs. (5), (6) and (18)) and in the virtual work (Eq. (7)) in the case of external excitation. Using Lagrange equations, a set of nonlinear ordinary differential equations is obtained; such system is then analysed by using numerical continuation methods.

5. Linear analysis: numerical results

Numerical analyses are carried out on three test cases described below:

Case A (*steel*): $L = 0.2\,\text{m}$; $R = 0.1\,\text{m}$; $h = 0.247 \times 10^{-3}\,\text{m}$; $\rho = 2796\,\text{kg/m}^3$; $\nu = 0.31$; $E = 71.02 \times 10^9\,\text{N/m}^2$.
Case B (*aluminium alloy*): $L = 0.2\,\text{m}$; $R = 0.2\,\text{m}$; $h = R/20$; $\rho = 7850\,\text{kg/m}^3$; $\nu = 0.3$; $E = 2.1 \times 10^{11}\,\text{N/m}^2$.
Case C (*PET+disk on the top*): Shell: $L = 0.096\,\text{m}$, $R = 0.044\,\text{m}$, $h = 0.3 \times 10^{-3}\,\text{m}$, $\rho = 1366\,\text{kg/m}^3$, $\nu = 0.4$, $E = 4.6 \times 10^9\,\text{N/m}^2$; Disk: $m = 0.82\,\text{kg}$, $J_y = J_z = 7.55 \times 10^{-4}\,\text{kg/m}^2$, $h_G = 0.01684\,\text{m}$.

5.1. Simply supported shells

For such simple case eigenfunctions are known: $U(x, \theta) = u_{k,n,c} \cos n\theta \cos k\eta$; $V(x,\theta) = v_{k,n,c} \sin n\theta \sin k\eta$; $W(x, \theta) = w_{k,n,c} \cos n\theta \sin k\eta$, where n is the number of nodal diameters and k is the number of longitudinal half waves; eigenfrequencies can be easily computed by solving a polynomial equation; as well as ratios $w_{k,n,c}/u_{k,n,c}$ and $w_{k,n,c}/v_{k,n,c}$ [1].

Analyses are carried out on Case A, the first 10 modes are evaluated by means of the exact theory, the present method (polynomials of degree 9) and the commercial software MSC Marc (480×50 elements, 480 in the circumferential and 50 in the longitudinal directions, element type CQUAD4), see Table 1.

It is remarkable that the shell exhibits a high modal density; there are 34 modes within the frequency range (484.6–1808 Hz), only the first 10 are shown; such high modal density is typical for cylindrical shells. The difference between exact theory and the present approach is negligible (beyond the fourth digit). The finite-element model gives accurate results, the error is less than 1%; however, this result has been obtained by means of a huge system having about 140 000 dof's; conversely, using the present approach, 22 dofs are needed, for obtaining up to the 34th mode, when polynomials of degree 9 are used. In Table 1 only four digits are used: this is the precision of MSC Marc output; therefore, for coherence, all results are reported with the

same precision. The present theory was test up to the 34th mode, similar accuracy was found; such results are not presented for the sake of brevity.

A second test is carried out on Case B, in order to check the accuracy of the polynomial expansion; in Table 1 the first five natural frequencies of axisymmetric modes are reported. In this case, polynomials used in the approximate method have degree equal to 15 ($M_U = 15$, $M_V = 15$, $M_W = 15$, $N_P = M_U + M_V + M_W - 5 = 40$). The accuracy is excellent, tests were carried out up to $k = 10$ (circular frequency $\omega_{10,1} = 61563 \times 2\pi$ rad/s), the error is below 5%; only results up to $k = 5$ are reported for the sake of brevity. In Table 1 only modes having a radially dominant vibration are considered, in order to check the convergence of the polynomial expansion; indeed, modes having a large number of longitudinal half waves are more difficult to simulate with polynomials.

For case B the fundamental mode is ($k = 1$, $n = 4$), the exact frequency is 2138.95 Hz; using polynomials of degree 5 (i.e. 10 dofs), we obtain 2139.19 Hz, the error is about 0.01%.

5.2. Clamped–clamped shells

The Case A shell is considered for this analysis; simulations are carried out by using the present theory (polynomials of degree 7) and the finite-element model having the same elements of the model described in the

Table 1
Simply supported shell, case A; comparison of natural frequencies: present theory vs. exact and finite-elements results (polynomials of degree 9)

Case	BC	Mode		Natural frequencies (Hz)				
				Exact frequency	Present theory		FEM	
		k	n		Freq.	Diff. %	Freq.	Diff. %
A	Simply	1	7	484.6	484.6	0	484.9	0.1
		1	8	489.6	489.6	0	490.0	0.1
		1	9	546.2	546.2	0	546.9	0.1
		1	6	553.3	553.3	0	553.7	0.1
		1	10	636.8	636.8	0	637.9	0.2
		1	5	722.1	722.1	0	722.5	0.1
		1	11	750.7	750.7	0	752.3	0.2
		1	12	882.2	882.2	0	884.6	0.3
		2	10	968.1	968.1	0	970.5	0.2
		2	11	983.4	983.4	0	985.9	0.3
B	Simply	1	0	4140.74	4140.77	0.001		
		2	0	4788.34	4788.66	0.007		
		3	0	6890.30	6891.43	0.016		
		4	0	10655.3	10657.7	0.023		
		5	0	15900.6	15904.7	0.026		
A	Clamped	1	9		687.7		685.4	0.3
		1	8		701.7		697.3	0.6
		1	10		727.9		727.2	0.1
		1	7		782		775.2	0.9
		1	11		809.2		809.7	0.1
		1	12		920.5		922.2	0.2
		1	6		939.6		930.1	1.0
		1	13		1055		1057	0.2
		2	11		1144		1143	0.1
		2	10		1172		1169	0.3

Simply supported shell, case B; comparison of axisymmetric modes natural frequencies: present theory vs. exact theory (only radial modes, w dominant, polynomials of degree 15). Clamped–clamped shell, case A; comparison of natural frequencies: present theory vs. exact and finite-elements results (polynomials of degree 7).

Table 2
Disk on the top, case C: comparison of natural frequencies: present theory vs. finite elements and experiments (polynomials of degree 9)

Geometry	Mode		Dimensionless frequency Ω	
R/h	$L/(mR)$	n	Present theory	3D elasticity [1]
20	2	0	0.93	0.95
20	2	1	0.57	0.55
20	2	2	0.33	0.34
20	2	3	0.24	0.26
20	2	4	0.27	0.26
20	0.5	0	1.11	1.08
20	0.5	1	1.1	1.09
20	0.5	2	1.06	1.05
20	0.5	3	1.03	1.05
20	0.5	4	1.03	1.00
500	2	2	0.33	0.32
500	2	4	0.12	0.12

previous section. No exact analytical results are available for such case. Modes up to 1260 Hz are analysed, i.e. the first 10 modes; in Table 1 natural frequencies are presented for comparison, k means that a mode has $k-1$ nodal circumferences (the meaning is similar to the simply supported case, even though the longitudinal displacement cannot be described by harmonic functions) and n is the number of nodal diameters. The agreement is excellent; indeed, the difference is less or equal to 1%. The number of dof's needed for describing a mode, using the present theory, is now 16.

5.3. Parametric analysis

In the present section, a parametric analysis is carried out to test the accuracy of the theory as the ratios R/h and L/R vary. Comparisons are carried out with results presented by Leissa [1] in nondimensional form and obtained using a 3D elasticity theory. Table 2 shows the nondimensional frequency $\Omega = \omega R\sqrt{\rho(1-\nu^2)/E}$ (ω is the natural frequency (rad/s)) as parameters R/h, $L/(mR)$, n vary, in the case of simply supported shells; m is the number of longitudinal half waves and n is the number of nodal diameters. Few digits are considered because in Ref. [1] results are presented in graphical form. This comparison confirms the accuracy of the present approach.

6. Experimental and theoretical results: disk on the top

The system under investigation is described in Figs. 2 and 3. A circular cylindrical shell, made of a polymeric material (PET, case C) is clamped at the base by gluing its bottom to a rigid support (a disk that is rigidly bolted to a shaker, such disk is technically called "fixture"); the connection is on the lateral surface of the shell, in order to increase the gluing surface, see Fig. 2. A similar connection is carried out on the top; in this case the shell is connected to a disk made of aluminium alloy, such a disk is not externally constrained; therefore, it induces a rigid body motion to the top shell end.

The use of PET is due to reasons that are beyond the purpose of the present paper. Indeed, the same set-up is used to perform experiments on dynamic instability, which gives rise to high amplitude of oscillation; in order to avoid plasticity for such high amplitudes, the PET polymer is considered. This polymer showed a good linear behaviour, both from elastic and dissipation point of view, as proven by excellent curve fittings obtained from experimental data. Material characteristics are directly measured with specific tests (E and ρ) or found in literature (ν).

The fixture is bolted to a high-power shaker (LDS V806, 9000N peak force, 100 g maximum acceleration, 300 kg payload, 1–3000 Hz band frequency); such shaker is used to excite the shell from the base or to provide a stiff support when the excitation is provided with different devices.

When the shell excitation is not furnished from the base, two kinds of excitation sources are applied: a micro-shaker (TIRAVIB, 10N peak force, see Fig. 3) or a micro-hammer.

As mentioned in the theoretical description, such case is much more complex than previous cases; the system exhibits both beam-like modes and shell-like modes (axisymmetric and asymmetric).

Experiments have been carried out by using different kinds of excitations; indeed, the system characteristics make difficult to excite all modes together. The first beam-like mode is excited using a shaker connected to the top disk, see Fig. 3, this kind of excitation allows to transfer energy to the shell through the rigid body motion of the top disk; the energy path will excite only modes having a rigid body motion of the top disk orthogonal to the shell axis, i.e. mainly beam modes. A second type of excitation is provided by exciting the shell from the base motion (Fig. 3); it was observed experimentally that such kind of excitation pumps energy to the first axisymmetric mode and to the second beam-like mode; other modes were scarcely excited. The third kind of excitation was carried out by means of a micro-hammer; such kind of excitation allows to furnish energy directly to shell modes having $n>1$. It is to note that the use of a micro-hammer allows to furnish a small amount of energy to the system; therefore, all modes for which the motion of the top disk is present ($n=0$ or 1) are not excited, because the energy pumped in the system is not enough to induce a disk motion detectable from sensors (accelerometers). The combination of three types of excitation allowed to identify all modes within the frequency range of interest.

About 80 measurement points were used for mode shape identification, with a uniform distribution over the shell; the classical FRF-based approach was used in lab experiments: when the shaker is used the excitation was fixed and several measurements were carried out by using one micro-accelerometer and moving it on several positions. Simultaneous measurements with several accelerometers were avoided in order to reduce the added mass effect. Each FRF was evaluated after performing several measurements (at least three) in order to reduce noise, a "curve fitting" allowed to identify frequencies, damping and mode shapes (see e.g. Ref. [16]).

In Table 3, experimental, analytical and finite-element results are presented: k means that the mode has $k-1$ nodal circumferences; n is the number of nodal diameters (beam modes can be considered $n=1$); FEM results are obtained by discretizing the shell similarly to the previous section; in this case also the top disk is discretized (brick elements) in order to check possible disk structural vibration. All modes are identified experimentally by using curve fitting techniques, present in LMS CADA-X, that give: frequency, modal damping ratio and modal shape. A 3D geometry of the system has been created before measurements, in order to associate each measurement to the corresponding point (and dof) on the geometry. The mode shape identification is of crucial importance in the case of shells; indeed, the high modal density makes difficult to compare experimental and theoretical/numerical modes using natural frequencies only; therefore, the visualization of modes is mandatory. Comparisons reported in Table 3 show that there is an excellent agreement among experiments, theory and finite elements. It is worthwhile to underline that finite-element results have been obtained after a heavy computation both from time computing and memory usage points of view.

In Fig. 6 mode shapes are reported both from experiments, theory and finite elements. The first mode (reprinted from Ref. [17]) is a beam-like mode; such kind of modes show both displacement and rotation of the top disk. The rotation is lost in the experiments because accelerometers are located radially in this set of measurements. In Ref. [17] beam modes were obtained both experimentally and theoretically, using a simplified approach for solving Sanders–Koiter equations; such approach did not give accurate results for higher-order modes. The second mode is axisymmetric, in this case the disk undergoes a pure translation motion. In the theoretical description of the second mode, some longitudinal ripples are visible, which are due to the accuracy used in computations. Indeed, the sharp variation of curvature at the ends is an edge effect particularly evident for the first axisymmetric mode; this induces some convergence problems in the polynomial expansion. However, such shape inaccuracy does not affect the frequency estimation. A final note is needed for shell-like modes ($n>1$): a micro-hammer and a micro-accelerometer have been used, the latter one is extremely light (0.25×10^{-3} kg); however, it induces a mass effect which causes an increasing of the radial deformation where the accelerometer is located. (Its position is fixed).

Results and comparisons presented in this section show that the analytical approach developed in the present work is capable to predict, with good accuracy, linear vibrations of circular cylindrical shells having different and complex boundary conditions.

Table 3
Comparison between the present theory and 3D elasticity results [1]: $\Omega = \omega R\sqrt{\rho(1-\nu^2)/E}$ (polynomials of degree 9)

Mode		Natural frequencies (Hz)				
		Experimental frequency	Present theory		Finite elements	
k	n		Frequency	Error (%)	Frequency	Error (%)
First beam-like mode, $n=1$		95	96	1.1	93	2.1
1	0	314	322	2.5	314	0
Second beam-like mode, $n=1$		438	432	2.5	424	3.2
1	6	791	797	0.8	782	1.1
1	7	816	802	1.7	802	1.7
1	5	890	888	0.2	885	0.6
1	8	950	926	2.5	918	3.4
1	9	1069	1016	5.0	1103	3.2

7. Nonlinear analysis: numerical results and comparisons

Large amplitude of oscillations are analysed for Case A shell; such geometry was deeply investigated in the past, see Refs. [18–21]. The shell is excited by means of a modally distributed force $q_r = f_{1,6}\sin(\eta)\cos(6\theta)\cos(\Omega t)$ (see also Eq. (7)) having amplitude equal to $f_{1,6} = 0.0012h^2\rho\omega_{1,6}^2$ and frequency close to the $(k=1,n=6)$ mode frequency: $\Omega \cong \omega_{1,6} = 2\pi \times 553.3\,\text{rad/s}$; the modal damping ratio considered in the calculations is 0.0005.

In expansions (24), the following modes having k longitudinal half waves and n nodal diameters, identified by (k,m), are selected: longitudinal displacement field, (1,0), (3,0), (1,6); circumferential displacement field, (1,6), (1,12), (3,12) and radial displacement field, (1,0), (3,0), (1,6). After selecting such modes, each expansion present in Eq. (16) is reduced to a three-terms expansion; the resulting dynamical system has 9 dof's.

In Fig. 7 the amplitude frequency curve is shown: this figure represents the maximum amplitude of vibration vs. the excitation frequency. Numerical results are obtained by means of the continuation software AUTO [22] that allows to find and follow periodic solutions of ordinary differential equations systems.

The response is slightly softening as confirmed by comparisons with Refs. [18–21]: the present model shows nonlinearity very close to Ref. [18]; Refs. [19–21] predict larger nonlinear softening behaviour. It is to note that in Refs. [20,21], Donnell's nonlinear shallow shell theory is considered: this theory is less accurate than Sanders–Koiter theory, the static condensation of in-plane displacements and simplified kinematics reduce the accuracy; generally, the Donnell's nonlinear shallow shell theory magnifies the softening behaviour.

It is worthwhile to stress that, in the past, several theoretical and numerical studies failed in predicting the correct nonlinear behaviour: often, spurious hardening behaviours were found. Recently, it was clarified that circular cylindrical shells generally show a softening behaviour [21]: only in very short or very thick shells one can observe hardening behaviour. Therefore, the analysis presented is Fig. 7 is an important benchmark for evaluating the accuracy of the method.

Note that the companion mode analysis has not been included in the model, because such deeper analysis is beyond the purposes of the present work.

8. Conclusions

In this work both theoretical and experimental analyses have been carried out on shells vibration. Linear and nonlinear vibrations of circular cylindrical shells are analysed by means of the Sanders–Koiter theory. The proposed method is based on a mixed expansion including both harmonic functions and orthogonal polynomials. The approach is effective in respecting complex boundary conditions as confirmed by several comparisons with experiments and finite-element methods. Comparisons between theory and experiments are

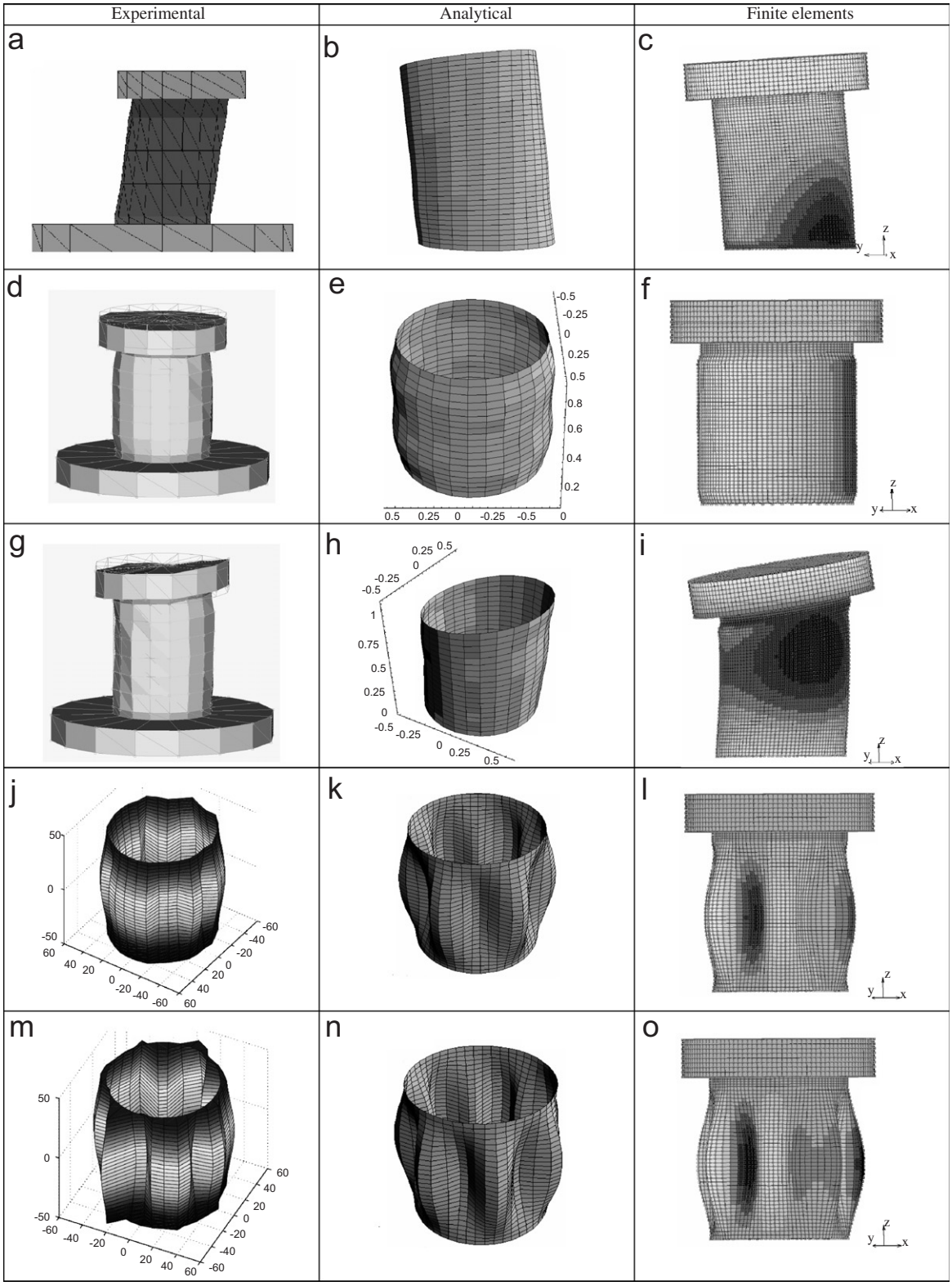

Fig. 6. Mode shape comparisons: (a, d, g, j, m) experiments; (b, e, h, k, n) present theory; (c, f, i, l, o) finite elements. (a–c) First beam-like mode $n = 1$ (95 Hz); (d–f) mode (1,0) (314 Hz); (g–i) second beam-like mode $n = 1$ (438 Hz); (j–l) mode (1,6) (791 Hz); (m–o) mode (1,7) (816 Hz). Mode shape (a) is reprinted from Ref. [17].

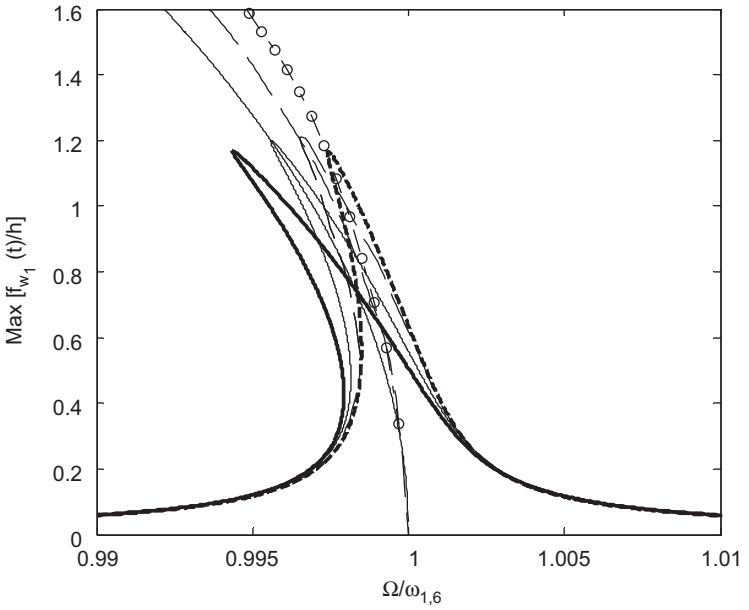

Fig. 7. Nonlinear response. '▬ ▬' present theory; '–○–' Ref. [18]; '— —' Ref. [19]; '—' Ref. [20]; '▬' Ref. [21].

carried out both on natural frequencies and mode shapes. The method has been tested in the case of large amplitude of vibration; also in this case the comparison with authoritative literature shows a good accuracy.

It is worthwhile to stress that the present approach shows good performances both in analysing complex boundary conditions and large-amplitude nonlinear vibrations. As underlined in the introduction, several interesting and accurate methods were developed in the past for analysing accurately linear vibrations of shells having complex shapes and boundary conditions; conversely, studies on nonlinear shell vibrations were generally focused on simple geometries and boundary conditions. Finally, nonlinear finite-elements codes are not yet reliable for carrying out parametric studies toward the understanding of the nonlinear scenario.

The present approach gives a general framework that allows to handle boundary conditions in a systematic way and attack nonlinear vibrations with a numerical efficiency largely higher and reliable than the finite-elements approach.

Acknowledgments

The author thank Prof. Amabili for scientific discussions and suggestions; Mr. Boglione and Mr. Vergnano for experiments.

References

[1] A.W. Leissa, *Vibration of Shells, NASA SP-288*, Government Printing Office, Washington, DC, 1993 (Now available from The Acoustical Society of America).

[2] M. Amabili, M.P. Païdoussis, Review of studies on geometrically nonlinear vibrations and dynamics of circular cylindrical shells and panels, with and without fluid-structure interaction, *Applied Mechanics Reviews* 56 (2003) 349–381.

[3] K.M. Liew, M.K. Lim, C.W. Lim, D.B. Li, Y.R. Zhang, Effects of initial twist and thickness variation on the vibration behaviour of shallow conical shells, *Journal of Sound and Vibration* 180 (2) (1995) 271–296.

[4] A. Bhaskar, P.C. Dumir, Non-linear vibration of orthotropic thin rectangular plates on elastic foundations, *Journal of Sound and Vibration* 125 (1) (1988) 1–11.

[5] K.M. Liew, T.Y. Ng, X. Zhao, Free vibration analysis of conical shells via the element-free kp-Ritz method, *Journal of Sound and Vibration* 281 (2005) 627–645.

[6] X. Zhao, T.Y. Ng, K.M. Liew, Free vibration of two-side simply-supported laminated cylindrical panels via the mesh-free kp-Ritz method, *International Journal of Mechanical Science* 46 (2004) 123–142.
[7] D. Zhou, Y.K. Cheung, S.H. Lo, F.T.K. Au, 3D vibration analysis of solid and hollow circular cylinders via Chebyshev–Ritz method, *Computer Methods in Applied Mechanics and Engineering* 192 (2003) 1575–1589.
[8] K.P. Soldatos, A. Messina, Vibration studies of cross-ply laminated shear deformable circular cylinders on the basis of orthogonal polynomials, *Journal of Sound and Vibration* 218 (2) (1998) 219–243.
[9] T.Y. Ng, L. Hua, K.Y. Lam, C.T. Loy, Parametric instability of conical shells by the generalized differential quadrature method, *International Journal for Numerical Methods in Engineering* 44 (1999) 819–837.
[10] K.Y. Lam, H. Li, T.Y. Ng, C.F. Chua, Generalized differential quadrature method for free vibration of truncated conical panels, *Journal of Sound and Vibration* 251 (2) (2002) 329–348.
[11] A.H. Nayfeh, H.N. Arafat, Nonlinear dynamics of closed spherical shells, *Proceedings of DETC2005 ASME 2005 International Design Engineering Technical Conferences & Computers and Information in Engineering Conference*, September 2005, Long Beach, CA, USA, paper N. DETC2005-85409.
[12] V.A. Trotsenko, Yu.V. Trotsenko, Methods for calculation of free vibrations of a cylindrical shell with attached rigid body, *Nonlinear Oscillations* 7 (2) (2004) 262–284.
[13] Y.V. Trotsenko, Frequencies and modes of vibration of a cylindrical shell with attached rigid body, *Journal of Sound and Vibration* 292 (2006) 535–551.
[14] N. Yamaki, *Elastic Stability of Circular Cylindrical Shells*, North-Holland, Amsterdam, 1984.
[15] M.A. Snyder, *Chebyshev Methods in Numerical Approximation*, Prentice-Hall, London, 1966.
[16] D.J. Ewins, *Modal Testing: Theory and Practice*, Wiley, New York, 1985.
[17] F. Pellicano, K.V. Avramov, Linear and nonlinear dynamics of a circular cylindrical shell connected to a rigid disk, *Communications in Nonlinear Science and Numerical Simulation* 12 (4) (2007) 496–518.
[18] M. Ganapathi, T.K. Varadan, Large amplitude vibrations of circular cylindrical shells, *Journal of Sound and Vibration* 192 (1) (1996) 1–14.
[19] J.C. Chen, C.D. Babcock, Nonlinear vibration of cylindrical shells, *AIAA Journal* 13 (7) (1975) 868–876.
[20] M. Amabili, F. Pellicano, A.F. Vakakis, Nonlinear vibrations and multiple resonances of fluid filled circular shells; part 1: equation of motion and numerical results, *Journal of Vibration and Acoustics* 122 (1) (2000) 346–354.
[21] F. Pellicano, M. Amabili, M.P. Païdoussis, Effect of the geometry on the non-linear vibration of circular cylindrical shells, *International Journal of Nonlinear Mechanics* 37 (2002) 1181–1198.
[22] E.J. Doedel, A.R. Champneys, T.F. Fairgrieve, Y.A. Kuznetsov, B. Sandstede, X. Wang, *AUTO 97: Continuation and Bifurcation Software for Ordinary Differential Equations* (*with HomCont*). Concordia University, Montreal, Canada, 1998.